Journal of Computational Physics **168,** 47–72 (2001)
doi:10.1006/jcph.2000.6678, available online at http://www.idealibrary.com on IDEAL®

A Computational Method for Eu's Generalized Hydrodynamic Equations of Rarefied and Microscale Gasdynamics

R. S. Myong

Division of Aerospace and Mechanical Engineering, Gyeongsang National University, Chinju, Gyeongnam 660-701, South Korea[1] *and Institute for Mathematics and Its Applications, University of Minnesota, 400 Lind Hall, 207 Church Street S.E., Minneapolis, Minnesota 55455*
E-mail: myong@nongae.gsnu.ac.kr

Received February 21, 2000; revised November 15, 2000

Generalized hydrodynamic equations have been proposed by Eu (*Kinetic Theory and Irreversible Thermodynamics*, 1992) for modeling the motion of gases far removed from equilibrium. His generalized hydrodynamic equations are consistent with the laws of thermodynamics. In this paper, a computational method of solving Eu's generalized hydrodynamic equations is presented. It has been shown that the new equations are applicable to all Mach numbers and indeed satisfy the second law of thermodynamics at all Knudsen numbers and to every order of approximation. The computational method of the generalized hydrodynamic equations is based on the finite-volume formulation and is exactly the same as the compressible Navier–Stokes codes, except for an additional routine for calculating the shear stress and the heat flux from the given conserved variables and thermodynamic forces. To check its validity and potential for hydrodynamics applications, the method is tested for the structure of one-dimensional shock wave and for a two-dimensional flat plate flow problem. The numerical results show that the new computational model yields the shock solutions for Mach numbers tested, up to $M = 30$, and removes the singularity near the leading edge of a flat plate that is ill-defined in the case of the Navier–Stokes theory.

Key Words: rarefied and microscale gasdynamics; generalized hydrodynamic equations; finite-volume method.

[1] Permanent address.

0021-9991/01 $35.00

1. INTRODUCTION

Hypersonic vehicles at high flight altitudes experience various flow regimes: continuum, slip, transitional, and free-molecular. Considerable parts of gas flows become highly nonequilibrium [20] because of the high Mach number and the low density, giving rise to a large Knudsen number. A similar situation, although from a different origin, namely, a small scale of the characteristic length, can be found in microscale gas flows; a typical example is internal flows in the channels of a microelectromechanical system (MEMS) [2, 19]. As a consequence of the high degree of nonequilibrium, the Navier–Stokes equations that are based on a small deviation from local equilibrium are inadequate for the aforementioned flow problems and new theoretical tools of analysis beyond the classical theory are necessary.

Much effort has been put into the development of such computational methods using hydrodynamic and kinetic approaches in the literature. One of the most successful methods is the so-called direct simulation Monte Carlo (DSMC) method [6, 32], and it has been used widely to investigate hypersonic rarefied gas flows. However, the computational cost is very high in the regime near the continuum limit because it is based on tracking a large number of statistically representative particles. To reduce the computational cost, hybrid methods which couple an Euler or Navier–Stokes solver with the DSMC method were proposed [33]. Even though these approaches can provide some benefits, there exist nontrivial issues to resolve if such approaches are to be successfully implemented: (1) when to switch between the continuum and molecular theory methods; and (2) how to pass information from one method to another so that an uninterrupted run of the solution procedure can be smoothly and continuously made.

However, there are computationally practicable methods that originate from the kinetic theory of gases and come under the general category of the moment method or the Chapman–Enskog method. These methods produce basically continuum hydrodynamic equations such as the Burnett equations [14, 22], the Grad's moment equations [16], the BGK–Burnett equations [3], the moment equations based on the Gaussian moment closure [7, 24, 25], and the moment equations derived by the so-called extended thermodynamics [28]. However, it is known that most of equations have difficulty ensuring that the second law of thermodynamics—one of the fundamental natural laws—is satisfied for all conditions of flow.[2] The absence of the consistency with the laws of thermodynamics in the aforementioned hydrodynamic approaches manifests itself in some defective behavior of the computed solutions with regard to some aspects of the flow problem, when either the shock-structure problem at a very high Mach number or the rapidly expanding flow [9] are considered.

In this study, we consider an alternative method such that the second law of thermodynamics is satisfied to every order of approximation or by whatever approximation made to the distribution function. This thermodynamic consistency requirement is enforced by identifying the quantity that is mathematically representative of the second law of thermodynamics. This quantity is called the calortropy, which reduces to the entropy known in equilibrium thermodynamics as the processes become reversible. In this regard it is useful to recall that in thermodynamics the entropy is defined for reversible processes only. This calortropy can be shown to obey a nonnegative inequality directly related to the H theorem

[2] For example, refer to papers [3, 9]. It is safe to say that the entropy production of the Burnett-type equations is not proved to be positive for all Knudsen numbers and flow conditions.

obeyed by the Boltzmann kinetic equation. The nonnegative inequality associated with the calortropy production provides us a thermodynamically consistent hydrodynamic equations for flow processes far removed from equilibrium. For further details of this line of theory the reader is referred to the original literature [12, 13]. The salient basic elements of the theory are the nonequilibrium canonical distribution function and the cumulant expansion for the Boltzmann collision term. Especially, the cumulant expansion may be regarded as a partial resummation of the expansion of the Boltzmann collision integral in a series of the Knudsen number, and as such, it takes into account highly nonlinear irreversible processes to infinite order. The first-order cumulant expansion takes a form of hyperbolic sine function whose argument is given in terms of basically a Rayleigh dissipation function. It turns out that the new equations possess an unusual feature that the two extreme regimes of rarefied and high density are adequately covered; in other words, that both free-molecular and continuum limits are uniformly described by the single formula of nonlinear dissipation function arising from the first-order cumulant expansion for the Boltzmann collision integral. The thermodynamically consistent set of hydrodynamic equations are called the generalized hydrodynamic equations, and were applied to calculate the shock profile for high Mach numbers, up to $M = 30$, in the works [1, 30]. It was shown that the results are comparable with the Monte Carlo simulation results and are in good agreement with experimental data.

There exists, however, a stiff challenge posed by Eu's generalized hydrodynamic equations as a computational tool for the simulation of gas flows in the multidimensional problem, because they are highly nonlinear and complex. It was found in the previous work [30] that the difficulty mainly resides in the complicated highly nonlinear form of the constitutive relations. The nonlinear terms, which appear in the form of a hyperbolic sine function, are intimately related to the calortropy production in the system. Because of the aforementioned nonlinear terms, it becomes apparent that the generalized hydrodynamic equations cannot be put into the hyperbolic system of partial differential equations, for which many numerical methods are available. For this reason, the constitutive equations, which are in the form of a nonlinear algebraic system and are coupled with the hyperbolic conservation laws, must be solved by an iterative method. Since the system involves six components of stress tensor and three components of heat flux vector, the computation will be very demanding. However, by observing that higher order variables (stress and heat flux) change far faster than the conserved variables, a method to overcome the computational difficulty can be found. The idea is to solve the constitutive equations with the conserved variables held constant since the conserved variables will remain constant on the time scale of change for the higher order variables such as the stress tensor and the heat flux.

In the present work we aim to develop an efficient multidimensional computational method for Eu's generalized hydrodynamic equations on the basis of the aforementioned idea, which is in essence the foundation of the so-called adiabatic approximation [12, 13]. This idea is in fact akin to the center manifold approximation [18]. Our interest here lies mainly in the development of a computational method for the generalized hydrodynamic constitutive equations, but not in a numerical method of the hyperbolic conservation laws. In particular, the main aim is to develop an efficient method for the calculation of the shear stress and the heat flux for multidimensional problems.

A key feature of the present computational method is that it is based on the hydrodynamic equations, which are proven to be consistent with the thermodynamic laws and compatible with the underlying macroscopic irreversible thermodynamics and at the same time are not restricted to small Knudsen numbers. In principle, it should yield solutions for all Knudsen

numbers and under any flow condition. Another feature is that the mathematical system of equations, like the Navier–Stokes equations, is of parabolic type. The parabolic type equations are used on the ground that it is very hard to find any preferential direction of propagation in high-order moments (stress and heat flux), contrary to the case with conserved variables whose evolution must be restricted by the hyperbolic conservation laws. Such choice is also motivated from previous studies where, except for certain extreme conditions, the Navier–Stokes equations are shown to remain surprisingly robust [21].

The present paper is organized as follows. First, some characteristic features of the generalized hydrodynamics are discussed vis à vis other mathematical models for gas transport in the nonlinear regimes. We then introduce a generalized hydrodynamic computational model and slip boundary conditions. In Section 4 a computational method is developed for solving the generalized hydrodynamic equations. Specific differences between the present method and previous methods will be discussed and pointed out. In the last section we present some numerical results in order to evaluate the present model and the conclusion is given.

2. MATHEMATICAL MODELS FOR RAREFIED AND MICROSCALE GAS TRANSPORT

In the nonlinear regime or processes occurring far removed from equilibrium, for example, in rarefied and microscale gas transport, the mean free path becomes comparable with the characteristic length of the system. As a result, the Knudsen number becomes large. Since the linear fluid dynamic approximations taken for the constitutive relations for the stress tensor and the heat flux in the classical hydrodynamics are valid in the regime of small Knudsen numbers, the Navier–Stokes equations become inadequate, and it is necessary to use mathematical models in which the microscopic molecular nature of gas is fully taken into account so that the large Knudsen number regime is properly accounted for. Such mathematical models range from the Boltzmann equation, the DSMC solutions, and the high-order fluid dynamic equations to either the deterministic equations of motion, which are solved by molecular dynamics methods, or probabilistic equations, such as the Klimontovich equation and the Liouville equation, which are solved by the Monte Carlo method. The fluid dynamic equations should be derived from the solution for the Boltzmann equation that in principle yields a theory of macroscopic irreversible processes compatible with thermodynamics, if proper care is exercised in solving the kinetic equation so as to satisfy the thermodynamic laws.

Mathematical models and solution methods for the description of the motion of gases are summarized in Fig. 1. Only the generalized hydrodynamic equations are taken for illustration, but other fluid dynamic equations may be used for a similar purpose. It can be easily seen from Fig. 1 that the Boltzmann equation plays a central role in the hierarchy of mathematical models. It was derived as an evolution equation for the singlet distribution function of a gas by considering the collision dynamics of two particles and combining it with a statistical assumption in the form of the molecular chaos. Since the molecular chaos assumption is not of a mechanical nature, the Boltzmann equation is not a purely mechanical equation of motion for a gas but should be regarded as a fundamental equation at the mesoscopic level of description of macroscopic processes in a dilute gas. Although it is a first-order differential equation in space and time, its solution becomes very complicated because it is nonlinear owing to the collision integral, which is made up of products of

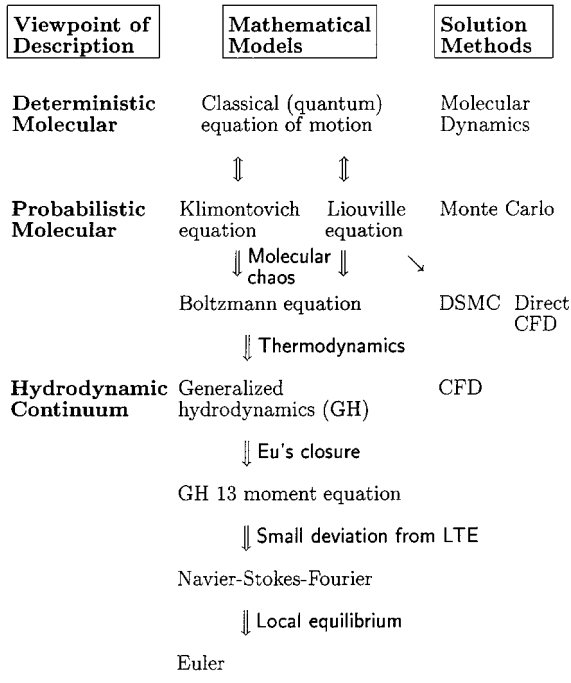

FIG. 1. Mathematical models and solution methods for the description of the motion of gases.

distribution functions. There can be an infinite number of solutions admissible for the kinetic equation, from which a thermodynamically compatible solution must be chosen. This means that given the Boltzmann equation as the kinetic equation the thermodynamics on the evolution of macroscopic variables are necessary to obtain the phenomenologically correct solution.

Conversely, the DSMC method is fundamentally different from solution methods of the Boltzmann equation in the sense that it is not based on any mathematical equations, but simulates directly the motion and interaction of particles. In essence, it starts from the Liouville equation and tracks down a large number of statistically representative particles by suitably taking into account the effect of particle collisions. Since this process corresponds to the introduction of the molecular chaos assumption, it is generally believed that the DSMC method is equivalent to solving the Boltzmann equation for a gas undergoing binary collisions.

The derivation of fluid dynamic equations from the Boltzmann equation begins with a realization that there exist three collision invariants in the Boltzmann equation: mass, total momentum, and energy. These are nothing but the hyperbolic conservation laws which can be also derived from the viewpoint of continuum mechanics. A difference can be found in methods to derive the equations of high-order terms, namely, the shear stress and the heat flux. There exist two basically different methods: the Chapman–Enskog method and the moment method. In the Chapman–Enskog method, the equations of high-order terms are derived by expanding the distribution functions, under the assumption of functional hypothesis, in series of Knudsen number and by substituting them into the Boltzmann equation to generate a hierarchy of equations, which are then sequentially solved. The hydrodynamic equations appear as the solvability conditions in this method. In the moment method, the hydrodynamic equations are obtained by expanding the distribution functions

in moments, and the evolution equations for moments are derived from the Boltzmann equations by using the macroscopic variables for the moments assumed. It turns out that both methods yield the Navier–Stokes equations as the first-order approximation for the nonconserved variables such as the stress tensor and the heat flux, but there remains a serious problem that the resulting high-order equations beyond the first order may not generally be consistent with the thermodynamic laws. One of the reasons for this problem is that the second law of thermodynamics is not fully incorporated into the formulations of these methods, even though the laws of thermodynamics govern macroscopic irreversible processes and play a critical role in yielding the phenomenologically correct solutions for the Boltzmann equation.

However, Eu's generalized hydrodynamics are derived in a way that the resulting equations are completely consistent with the second law of thermodynamics to every order of approximations that may be taken. As in the moment method, distribution functions are assumed to evolve as functionals of macroscopic moments, but their flux dependence is derived from a careful examination of the H theorem as well as the calortropy production associated with the H theorem. For the detailed discussion of the subtlety of the Boltzmann kinetic theory and Eu's generalized hydrodynamics, the reader is referred to his original work [10, 12, 13].

3. EU'S GENERALIZED HYDRODYNAMIC EQUATIONS

3.1. *Governing Equations*

A thermodynamically consistent hydrodynamic computational model of the conserved and nonconserved variables has been developed by Myong [30] on the basis of Eu's generalized hydrodynamic equations. If the following dimensionless variables and parameters are used,

$$t^* = t/(L/u_r), \quad \mathbf{x}^* = \mathbf{x}/L, \quad \eta^* = \eta/\eta_r, \quad \lambda^* = \lambda/\lambda_r, \quad \mathbf{u}^* = \mathbf{u}/u_r, \quad \rho^* = \rho/\rho_r,$$
$$T^* = T/T_r, \quad p^* = p/p_r, \quad E^* = E/u_r^2, \quad \mathbf{\Pi}^* = \mathbf{\Pi}/(\eta_r u_r/L), \quad \mathbf{Q}^* = \mathbf{Q}/(\lambda_r \triangle T/L T_r),$$

the dimensionless evolution equations of a monatomic gas in the generalized hydrodynamics can be written as

$$\frac{\partial \mathbf{U}}{\partial t} + \nabla \cdot \mathbf{F}_T = 0, \tag{1}$$

and

$$\hat{\mathbf{\Pi}}\, q(c\hat{R}) = \hat{\mathbf{\Pi}}_0 + [\hat{\mathbf{\Pi}} \cdot \nabla \hat{\mathbf{u}}]^{(2)}, \tag{2}$$
$$\hat{\mathbf{Q}}\, q(c\hat{R}) = \hat{\mathbf{Q}}_0 + \hat{\mathbf{\Pi}} \cdot \hat{\mathbf{Q}}_0. \tag{3}$$

Here, $\hat{\mathbf{\Pi}}_0$ and $\hat{\mathbf{Q}}_0$ are determined by the Newtonian law of viscosity and the Fourier law of heat conduction, respectively:

$$\mathbf{\Pi}_0 = -2\eta[\nabla \mathbf{u}]^{(2)}, \quad \mathbf{Q}_0 = -\lambda \nabla \ln T.$$

The asterisks are omitted from the aforementioned equations for the notational brevity,

$$\mathbf{U} = \begin{pmatrix} \rho \\ \rho\mathbf{u} \\ \rho E \end{pmatrix},$$

$$\mathbf{F} = \begin{pmatrix} \rho\mathbf{u} \\ \rho\mathbf{u}\mathbf{u} + \frac{1}{\gamma M^2} p\mathbf{I} \\ \left(\rho E + \frac{1}{\gamma M^2} p\right)\mathbf{u} \end{pmatrix}, \quad \mathbf{F}_v = \frac{1}{\mathrm{Re}} \begin{pmatrix} 0 \\ \mathbf{\Pi} \\ \mathbf{\Pi}\cdot\mathbf{u} + \frac{1}{\mathrm{EcPr}}\mathbf{Q} \end{pmatrix},$$

$$\hat{\mathbf{\Pi}} \equiv \frac{N_\delta}{p}\mathbf{\Pi}, \quad \hat{\mathbf{Q}} \equiv \frac{N_\delta}{p}\frac{\mathbf{Q}}{\sqrt{T/(2\epsilon)}},$$
$$\nabla\hat{\mathbf{u}} \equiv -2\eta\frac{N_\delta}{p}\nabla\mathbf{u}, \quad \epsilon \equiv \frac{1}{\mathrm{PrEc}T_r/\triangle T},$$

and $q(c\hat{R})$ is a nonlinear factor defined by

$$q(c\hat{R}) = \frac{\sinh(c\hat{R})}{c\hat{R}},$$
$$\hat{R}^2 \equiv \hat{\mathbf{\Pi}}\colon\hat{\mathbf{\Pi}} + \hat{\mathbf{Q}}\cdot\hat{\mathbf{Q}}.$$

The $\mathbf{U}$ is the vector made up of conserved variables and $\mathbf{F}_T$ represents the sum of the inviscid flux vector $\mathbf{F}$ and the viscous flux vector $\mathbf{F}_v$. The $\mathbf{\Pi}$ and $\mathbf{Q}$ represent the shear stress and the heat flux, respectively. The symbol $[\nabla\mathbf{u}]^{(2)}$ stands for the traceless symmetric part of tensor $\nabla\mathbf{u}$ and the term $[\mathbf{\Pi}\cdot\nabla\mathbf{u}]^{(2)}$ represents the traceless symmetric part of the coupling between the shear stress and velocity gradient tensor. It should be mentioned that in the present study the term $(\hat{\mathbf{Q}}\cdot\nabla\hat{\mathbf{u}})/2\mathrm{Pr}$ appearing in the original constitutive relation of heat flux [30] is omitted from the constitutive relation (3) for the sake of simplicity. The M, Re, Ec, and Pr are dimensionless fluid dynamic numbers: Mach, Reynolds, Eckert, and Prandtl numbers, respectively. The caret $\hat{}$ over a symbol represents a quantity with the dimension of the ratio of the stress to the pressure. The subscript r stands for the reference state; for example, the state of the inflow condition. The constant c, which is given by

$$c = \left[\frac{2\sqrt{\pi}}{5}A_2(\nu)\Gamma[4 - 2/(\nu - 1)]\right]^{1/2}, \tag{4}$$

has a value between 1.0138 (Maxwellian) and 1.2232 ($\nu = 3$), where ν is the exponent of the inverse power law for the gas particle interaction potential. The $A_2(\nu)$ is a pure number; its tabulated values are available in the monographs on kinetic theory [8]. The η and λ are the Chapman–Enskog viscosity and thermal conductivity. They can be expressed as $\eta = T^s,\ \lambda = T^{s+1}$ where $s = \frac{1}{2} + 2/(\nu - 1)$.

For a monatomic gas, $\gamma = \frac{5}{3}$ and $\mathrm{Pr} = \frac{2}{3}$. For a perfect gas, the following dimensionless relations hold:

$$p = \rho T, \quad \rho E = \frac{p/\gamma M^2}{\gamma - 1} + \frac{1}{2}\rho\mathbf{u}\cdot\mathbf{u}. \tag{5}$$

A composite number, which is defined by

$$N_\delta \equiv \frac{\eta_r u_r / L}{p_r} = \gamma \frac{M^2}{\mathrm{Re}} = \mathrm{Kn} M \sqrt{\frac{2\gamma}{\pi}},$$

measures the magnitude of the viscous stress relative to the hydrostatic pressure, so that it indicates the degree of departure from equilibrium. It should be emphasized that terms in the present constitutive relations appear multiplied by the composite number N_δ. Through this number the new hydrodynamic Eqs. (1)–(3) take into account the effects of high Knudsen and Mach numbers. As N_δ becomes small, the Navier–Stokes–Fourier constitutive relations are recovered from the constitutive relations (2) and (3):

$$\mathbf{\Pi} = \mathbf{\Pi}_0 \quad \text{and} \quad \mathbf{Q} = \mathbf{Q}_0. \tag{6}$$

The unique feature of the new set of hydrodynamic equations is the existence of a highly nonlinear factor $q(c\hat{R})$ in the constitutive relations. It depends on a parameter $\hat{R}$, which is directly related to the Rayleigh dissipation function and gives a measure of departure from equilibrium. This nonlinear factor $q(c\hat{R})$ describes the mode of energy dissipation accompanying the irreversible processes and directly related to the calortropy production in the system [12]:

$$\sigma_{\mathrm{ent}} \sim \hat{R}^2 q(c\hat{R}). \tag{7}$$

Since $\hat{R}^2$, which is the sum of the double contraction of stress tensors and the dot product of heat flux vectors, and $q(c\hat{R})$ always remain positive, σ_{ent} is inherently positive regardless of the value of the Knudsen number, the order of approximations, and flow conditions.

Another feature is that the new equations are frame-independent; in other words, they are not dependent on the motion of the observer. This is related to the fact that the generalized hydrodynamic equations can be made corotational by using the Jaumann derivative [11]. Not all of the previously mentioned hydrodynamic equations satisfy such property, whereas the Navier–Stokes equations always do.[3]

3.2. *Boundary Conditions*

The hydrodynamic Eqs. (1)–(3) are subject to boundary conditions. The common practice in rarefied and microscale gasdynamics is to employ some type of slip boundary conditions, for example, the Maxwell–Smoluchowski condition. Although this slip boundary condition turns out to be satisfactory for many problems, there exists growing evidence [2] that it plays a crucial role in determining the overall flowfield in microscale gas flows. It is based on the notion of accommodation coefficients which measure the slip effects at the solid boundary, depending on the gradient of tangential velocity and temperature. Under the assumption of uniform temperature, it can be simplified as

$$u = u_w + \frac{(2-\sigma)}{\sigma} l \left(\frac{\partial u}{\partial n} \right)_w. \tag{8}$$

[3] There remains the general question of whether constitutive relations should be frame-independent or not. It was, however, generally accepted that correctly formulated constitutive relations were necessarily frame-independent [37].

The subscript w stands for the wall and l is the mean free path. The slip velocity depends on the mean free path, that is, the Knudsen number, accommodation coefficients σ, and the normal gradient of the tangential velocity. The case of $\sigma = 1$ represents perfect diffusive reflection. However, it should be noticed that the slip velocity is unbounded since either the value of the Knudsen number or the normal gradient of the tangential velocity can be very large.[4]

It is also instructive to mention that owing to the presence of an adjustable coefficient σ this condition loses the predictability. Consequently, handling the boundary condition for high-Knudsen-number gas flows becomes problem-dependent. Some calculations indicated that the general solutions were highly dependent on the exact value of surface accommodation coefficients [26] used.

In the present study, a new boundary condition is considered that not only recovers the predictability but also facilitates a hydrodynamic treatment of the entire density regime with a single formalism. It is expected that the present method can avoid the problems inherent to the Maxwell–Smoluchowski condition. The present method takes the interfacial gas–surface molecule interaction into account. A fraction α of molecules reaching thermal equilibrium with the wall can be expressed, in the dimensional form, as [5, 29]

$$\alpha = \frac{\beta p}{1 + \beta p}, \tag{9}$$

where the parameter β depends on the wall temperature T_w and the interfacial interaction parameters. By imagining the gas–surface molecule interaction process as a chemical reaction, it is possible to express the parameter β in the form

$$\beta = \frac{A l_r}{k_B T_w} \exp\left(\frac{D_e}{k_B T_w}\right) \cdot \frac{\ell}{l_r}, \tag{10}$$

where k_B is the Boltzmann constant, and where A is the mean area of a site and D_e is the potential parameter. These parameters can be inferred from experimental data or theoretical consideration of intermolecular forces and the surface–molecule interaction. The subscript r stands for the reference value such as the value at the free-stream or the local value adjacent to the surface, and ℓ is a mean collision distance between the wall surface and the gas molecules at all angles [5]. When the characteristic length L is taken equal to ℓ, the ℓ / l_r is equivalent to $1/\mathrm{Kn}$. When the free-stream mean free path is taken as ℓ, it becomes unity. With α so calculated, the boundary values of temperature and velocity can be determined by the weighted means

$$T = \alpha T_w + (1 - \alpha) T_r, \tag{11}$$

$$u = \alpha u_w + (1 - \alpha) u_r. \tag{12}$$

In the multidimensional problem, u should be interpreted as the magnitude of the velocity vector. In contrast to the Maxwell–Smoluchowski boundary condition the new boundary condition does not involve the gradient of velocity and is always bounded by the reference value; this seems to be physically more sensible. A simple expression for β can be obtained

[4] A general velocity slip boundary condition has been developed by Beskok and Karniadakis [4] that remains bounded for all Knudsen numbers. It must be, however, noted that there still exists a possibility of unboundness from a small σ or from a large gradient of tangential velocity.

after some manipulation,

$$\beta = \sqrt{\frac{\pi}{32}}\frac{A}{c^2 d_{\mathrm{STP}}^2}\left[\frac{T_r}{273}\right]^{\frac{2}{\nu-1}}\frac{T_r}{T_w}\exp\left(\frac{D_e}{k_B T_w}\right)\frac{\ell}{l_r}\cdot\frac{1}{p_r}, \tag{13}$$

where d represents the diameter of the molecule. In deriving the Eq. (13) from (10), in addition to the equation of state and the definition of c given in (4), the relations

$$l = \sqrt{\frac{\pi}{2}}\frac{\eta}{\rho\sqrt{RT}},$$

$$\eta = \frac{5}{8A_2(\nu)\Gamma[4-2/(\nu-1)]d^2}\sqrt{\frac{mk_BT}{\pi}},$$

$$d = \left(\frac{K}{2k_BT}\right)^{\frac{1}{\nu-1}},$$

were used, where m is the molecular mass and K is the coefficient of the inverse power law of interaction. For an Ar–Al molecular interaction model,

$$D_e = 1.32\,\mathrm{kcal/mol}, \quad A = 5\times10^{-15}\,\mathrm{cm}^2, \quad d_{\mathrm{STP}} = 3.659\times10^{-8}\,\mathrm{cm}.$$

The parameter β reduces to

$$\beta = 1.1294\left(\frac{T_r}{273}\right)^{\frac{1}{4}}\frac{T_r}{T_w}\exp\left(\frac{664.23}{T_w}\right)\frac{\ell}{l_r}\cdot\frac{1}{p_r}.$$

In Fig. 2 the fraction of molecules reaching thermal equilibrium in the gas–surface interface as a function of pressure is plotted in logarithmic scale.

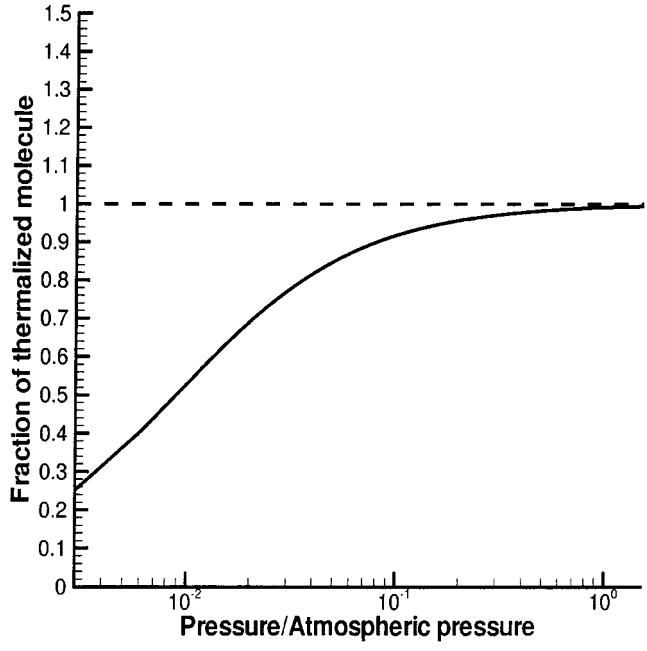

FIG. 2. Fraction of molecules reaching thermal equilibrium in the interface as a function of pressure in logarithmic scale ($\ell = L = 1\ \mu$m, $T_w = 300$ K).

In summary, the fraction α of molecules reaching equilibrium depends on the Knudsen number, free-stream and wall temperature, exponent of the inverse power laws ν, and gas–surface parameters D_e and A. With an interfacial gas–surface molecule interaction model the present generalized hydrodynamic equations require no more conditions beyond the boundary conditions of the Navier–Stokes equations.

4. CFD ALGORITHMS

The generalized hydrodynamic Eqs. (1)–(3), as is the case for the well-documented Navier–Stokes equations, must satisfy the collision-free hyperbolic conservation laws,

$$\frac{\partial}{\partial t}\int_V \mathbf{U}\, dV + \oint_S \mathbf{F}_T \cdot \mathbf{n}\, dS = 0,$$

where S represents the bounding surface of the control volume V. Here it should be emphasized that these laws are the exact consequence of both kinetic theory and continuum mechanics. Only after some approximations are made to nonconserved variables (stress and heat flux), do they become approximate fluid dynamic equations. Therefore, most of modern CFD schemes based on the hyperbolic conservation laws can be applied to treating these equations. In the present study, the upwind scheme with van Leer's flux vector splitting solver [35] is used. The one-dimensional discretized form of the hyperbolic conservation laws in the finite volume formulation can be expressed as

$$\mathbf{U}_i^{n+1} = \mathbf{U}_i^n - \frac{\triangle t}{\triangle x}\left[\mathbf{F}^n_{T_{i+\frac{1}{2}}} - \mathbf{F}^n_{T_{i-\frac{1}{2}}}\right], \tag{14}$$

where $\mathbf{U}$ is the cell-averaged conserved variables, $\triangle x$ is the size of i-cell, $\triangle t$ is the time step, and $\mathbf{F}_T$ is the numerical flux function which gives the flux through cell interfaces. Note that in the finite volume formulation the shear stress and heat flux are defined only on cell surfaces. Second-order accuracy can be obtained by using the MUSCL–Hancock method [36].

4.1. *Main Features*

Together with these algorithms on the conservation laws (1), an algorithm to solve the nonlinear algebraic system of constitutive relations (2) and (3) must be developed. It should provide the shear stress and heat flux, which are essential to define the numerical flux through cell interfaces. In the present work, they will be solved by an iterative method for given thermodynamic variables (pressure and temperature) and the gradients of velocity and temperature.

This process is trivial in the Navier–Stokes equations since the shear stress and heat flux can be eliminated from the hyperbolic conservation laws. The resulting laws involve only the conserved variables and thermodynamic forces of the gradient of velocity and temperature.

The situation, however, becomes very different in the case of other high-order moment equations. For example, in the case of the moment equations based on the extended thermodynamics, the constitute equations are derived in a way that the whole system is of hyperbolic type. Thus the numerical algorithm based on the hyperbolic conservation laws is applied not only to the conserved variables but also to higher order variables such as the stress and the heat flux. As a result, the aforementioned moment methods do not require

any procedure to solve the algebraic equations but must solve a hyperbolic system with more variables, for example, the 35-moment equations in the case of Ref. [7]. In practice, they also require a wall boundary condition for higher order variables, which often becomes difficult to determine, if not impossible.

From this consideration, it becomes apparent that the present numerical method shares more common features with the Navier–Stokes method than with other moment methods. It is based on the hyperbolic system with five components of conserved variables. An additional step is needed only when stress and heat flux appearing in the flux of the system are calculated from the nonlinear algebraic constitutive equations.

4.2. *Solutions of Constitutive Relations*

In general, the constitutive Eqs. (2) and (3) consist of nine equations of (Π_{xx}, Π_{xy}, Π_{xz}, Π_{yy}, Π_{yz}, Π_{zz}, Q_x, Q_y, Q_z) for known 14 parameters (p, T, ∇u, ∇v, ∇w, ∇T). Because of the highly nonlinear terms, it is, however, not obvious how to develop a proper numerical method for solving the equations. Nevertheless, it was shown [30] that they can be solved by a numerical method in the case of a one-dimensional problem.

In the case of a two-dimensional problem the stress and heat flux components (Π_{xx}, Π_{xy}, Q_x) on a line in the two-dimensional physical plane induced by thermodynamic forces (u_x, v_x, T_x) can be approximated as the sum of two solvers: (1) one on (u_x, 0, T_x) and (2) another on (0, v_x, 0). In the three-dimensional problem, (Π_{xx}, Π_{xy}, Π_{xz}, Q_x) on a surface can be approximated as the sum of two solvers: (1) one on (u_x, 0, 0, T_x) and (2) another on (0, v_x, w_x, 0). Here we present only the two-dimensional case because it can be easily extended to the three-dimensional problem by noting $(v_x, w_x) = (v\cos\theta, v\sin\theta)$ where

$$v = \sqrt{v_x^2 + w_x^2}, \quad \theta = \tan^{-1}\frac{w_x}{v_x}.$$

In the previous work [30], it was shown that the equations for the first solver are given by

$$\hat{\Pi}_{xx} q(c\hat{R}) = (\hat{\Pi}_{xx} + 1)\hat{\Pi}_{xx_0}, \tag{15}$$

$$\hat{Q}_x q(c\hat{R}) = (\hat{\Pi}_{xx} + 1)\hat{Q}_{x_0}, \tag{16}$$

where

$$\hat{R}^2 = \frac{3}{2}\hat{\Pi}_{xx}^2 + \hat{Q}_x^2.$$

The factor $3/2$ in $\hat{R}^2$ originates from the symmetry relation

$$\hat{\Pi}_{yy} = \hat{\Pi}_{zz} = -\frac{1}{2}\hat{\Pi}_{xx}.$$

The equations for the second solver are given in the form

$$\hat{\Pi}_{xx} q^2(c\hat{R}) = -\frac{2}{3}(\hat{\Pi}_{xx} + 1)\hat{\Pi}_{xy_0}^2, \tag{17}$$

where

$$\hat{R}^2 = 3\hat{\Pi}_{xx}(\hat{\Pi}_{xx} - 1),$$

which follows from the symmetry relation

$$\hat{\Pi}_{xx} = \hat{\Pi}_{zz} = -\frac{1}{2}\hat{\Pi}_{yy}$$

and the constraint

$$\hat{\Pi}_{xy} = \mathrm{sign}\big(\hat{\Pi}_{xy_0}\big)\left[-\frac{3}{2}(\hat{\Pi}_{xx}+1)\hat{\Pi}_{xx}\right]^{1/2}. \tag{18}$$

These can be solved by the method of iteration, which turned out to provide converged solutions within a few iterations. For mathematical proof of convergence, the reader is referred to the previous work [30]. The iteration procedures can be summarized as follows. In the solver on $(u_x, 0, T_x)$, for positive $\hat{\Pi}_{xx}$ and $\hat{Q}_x$,

$$\hat{R}_{n+1} = \frac{1}{c}\sinh^{-1}\left[c\big(\hat{\Pi}_{xx_n}+1\big)\hat{R}_0\right]$$

and

$$\frac{\hat{Q}_{x_{n+1}}}{\hat{\Pi}_{xx_{n+1}}} = \frac{\hat{Q}_{x_n}}{\hat{\Pi}_{xx_n}} = \frac{\hat{Q}_{x_0}}{\hat{\Pi}_{xx_0}},$$

and for negative $\hat{\Pi}_{xx}$ and $\hat{Q}_x$,

$$\hat{\Pi}_{xx_{n+1}} = \frac{\hat{\Pi}_{xx_0}}{q(c\hat{R}_n) - \hat{\Pi}_{xx_0}}$$

and

$$\hat{Q}_{x_{n+1}} = \frac{\big(\hat{\Pi}_{xx_n}+1\big)\hat{Q}_{x_0}}{q(c\hat{R}_n)}.$$

In these expressions, $\hat{\Pi}_{xx_1}$ and $\hat{Q}_{x_1}$ are given by the equations

$$\hat{\Pi}_{xx_1} = \frac{\sinh^{-1}(c\hat{R}_0)}{c\hat{R}_0}\,\hat{\Pi}_{xx_0},$$

$$\hat{Q}_{x_1} = \frac{\sinh^{-1}(c\hat{R}_0)}{c\hat{R}_0}\,\hat{Q}_{x_0}.$$

In the solver on $(0, v_x, 0)$, the $\hat{\Pi}_{xx}$ can be obtained for a given $\hat{\Pi}_{xy_0}$ through the equation

$$\hat{\Pi}_{xx_{n+1}} = -\frac{\hat{\Pi}_{xy_0}^2}{3q^2(c\hat{R}_n)/2 + \hat{\Pi}_{xy_0}^2}.$$

The $\hat{\Pi}_{xy}$ can be calculated by using the constraint (18).

The general properties of constitutive relations are shown in Fig. 3a, and 3b. Figure 3a shows the asymmetry of the normal stress for rapid expansion and compression of gas. In this figure the heat flux is assumed to be equal to zero for the sake of simplicity. It has been reported that the augmented conventional Burnett equations produce a severe instability

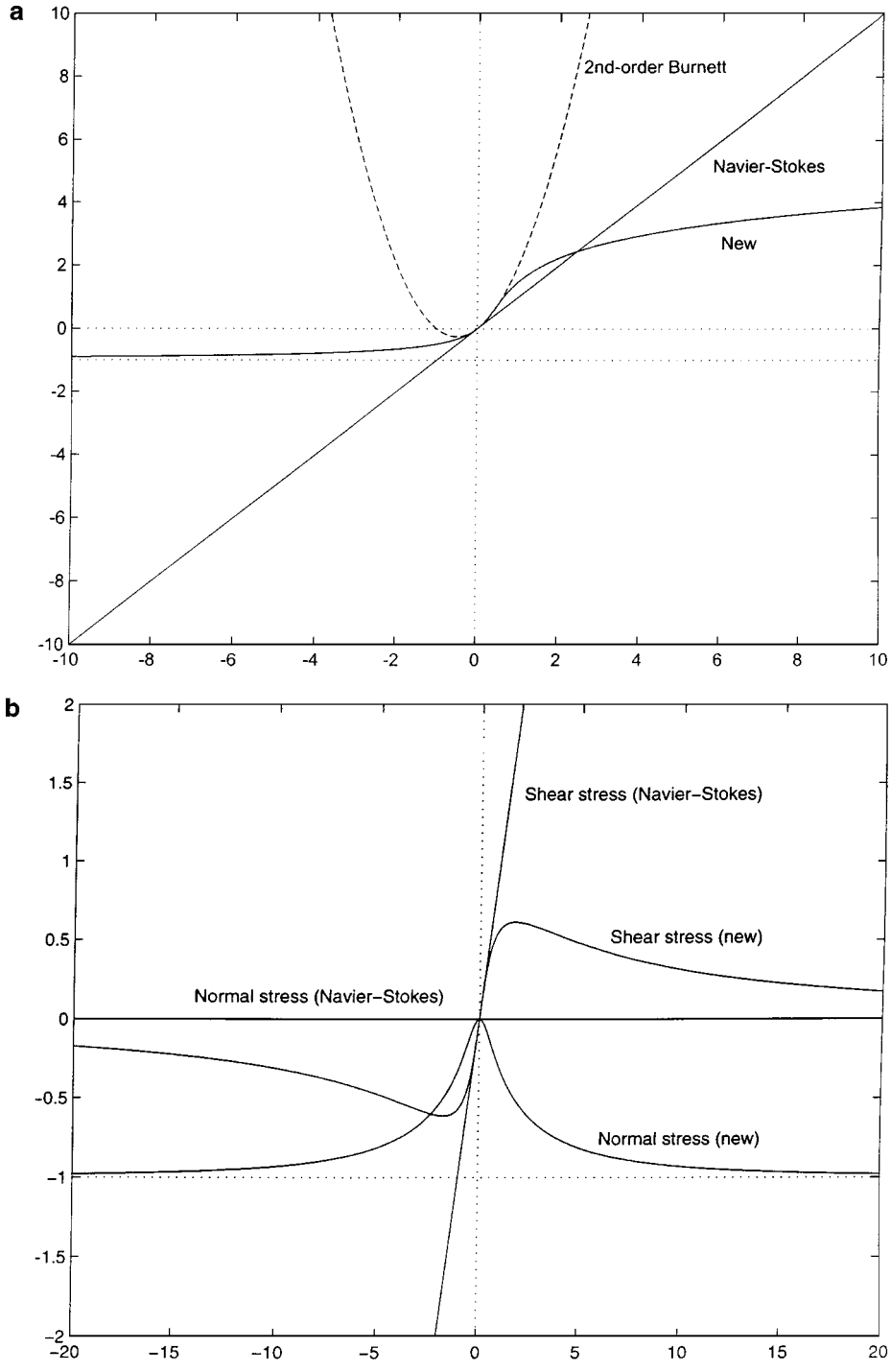

FIG. 3. (a) Generalized hydrodynamics, and second-order Burnett constitutive relations relative to the Navier–Stokes relations (argon, u_x only, no heat flux). The horizontal and vertical axes represent the Navier–Stokes relations $\hat{\Pi}_{xx_0}$ and the relations $\hat{\Pi}_{xx}$, respectively. The gas is expanding in the range of $\hat{\Pi}_{xx_0} < 0$, whereas the gas is compressed in the range of $\hat{\Pi}_{xx_0} > 0$. (b) Generalized hydrodynamic constitutive relations relative to the Navier–Stokes relations (argon, v_x only). The horizontal axis represents the velocity gradient $\hat{v}_x/2$ or $\hat{\Pi}_{xy_0}$. The vertical axis represents the normal ($\hat{\Pi}_{xx}$) and shear ($\hat{\Pi}_{xy}$) stresses.

near the point where the flow separates at the shoulder of the hypersonic vehicles [27]. It was suggested that the instability is caused by the problems that a rapidly expanding gas exhibits a negative entropy production (more properly, the calortropy production) in the Burnett-type formulations. The origin of the instability can be explained by examining the second-order Burnett equation (u_x only)

$$\hat{\Pi}_{xx} = \left(\hat{\Pi}_{xx_0} + 1\right)\hat{\Pi}_{xx_0}.$$

The corresponding entropy production [9], which can be written in the one-dimensional problem as

$$\sigma_{\text{ent}} \sim \frac{\eta}{T}\left(\frac{\partial u}{\partial x}\right)^2\left[1 - \frac{5\eta}{3p}\frac{\partial u}{\partial x}\right],$$

can be negative when the gas is rapidly expanding, or when

$$\hat{\Pi}_{xx_0} < -\frac{6}{5}.$$

The loss of one-to-one correspondence in Fig. 3a is a sign of such nonphysical behavior. By contrast, the new relations will not suffer such an unphysical feature since they always yield positive calortropy production.

Figure 3b demonstrates that $(\hat{\Pi}_{xx} + 1)$ or $(\Pi_{xx} + p/N_\delta)$, as well as $\hat{\Pi}_{xy}$ of the new relations, approach zero as the tangential velocity gradient becomes very large. Such an asymptotic behavior indicates that the new relations have a correct free-molecular limit, implying that the velocity-slip phenomenon caused by the non-Newtonian effect can be explained in purely hydrodynamic terms. The details of properties of the new constitutive relations are given in the previous work [30].

4.3. *Numerical Flux in the Finite Volume Formulation*

The numerical flux through the interface in the Eq. (14) in general non-Cartesian domains can be determined by exploiting the rotational invariance of the conservation laws. Let us consider the l-th intercell boundary $\triangle L_l$ of finite area $A_{i,j}$ in two-dimensional (x, y) space. Let $(\mathbf{n}, \mathbf{s})_l$ be the outward unit vector normal to the l-th boundary, and let the unit vector be tangent to the l-th boundary with the convention that the interior of the volume always lies on the left-hand side of the boundary. If θ_l is defined as the angle formed by the x-direction and the normal vector $\mathbf{n}_l$, it can be shown that the Eq. (14) becomes

$$\mathbf{U}_{i,j}^{n+1} = \mathbf{U}_{i,j}^{n} - \frac{\triangle t}{A_{i,j}}\sum_{l=1}^{N}\mathbf{R}_l^{-1}\mathbf{F}_{T_l}^{n}\triangle L_l, \tag{19}$$

where

$$\mathbf{U}_{i,j} = \begin{pmatrix} \rho \\ \rho u \\ \rho v \\ \rho E \end{pmatrix}_{i,j},$$

$$\mathbf{F}_l = \begin{pmatrix} \rho u_n \\ \rho u_n^2 + \frac{1}{\gamma M^2} p \\ \rho u_n u_s \\ \left(\rho E + \frac{1}{\gamma M^2} p\right) u_n \end{pmatrix}_l, \quad \mathbf{F}_{v_l} = \frac{1}{\mathrm{Re}} \begin{pmatrix} 0 \\ \Pi_{nn} \\ \Pi_{ns} \\ \Pi_{nn} u_n + \Pi_{ns} u_s + \frac{1}{\mathrm{EcPr}} Q_n \end{pmatrix}_l,$$

and $\mathbf{R}_l \equiv \mathbf{R}(\theta_l)$ is the rotation matrix, namely,

$$\mathbf{R}(\theta) = \begin{pmatrix} 1 & 0 & 0 & 0 \\ 0 & \cos\theta & \sin\theta & 0 \\ 0 & -\sin\theta & \cos\theta & 0 \\ 0 & 0 & 0 & 1 \end{pmatrix}.$$

The N is the number of interfaces in a cell. In this process a transformation law between the components of the tensor in the (x, y) coordinates ($\mathbf{\Pi}$) and the components of the tensor in the (n, s) coordinates ($\tilde{\mathbf{\Pi}}$) is used [15]:

$$\mathbf{\Pi} = \mathbf{R}^{-1} \tilde{\mathbf{\Pi}} \mathbf{R}. \tag{20}$$

The extension to the three-dimensional problem is also straightforward. Consider the l-th intercell surface boundary $\triangle S_l$ of finite volume $V_{i,j,k}$ in three-dimensional (x, y, z) space. Let $(\mathbf{n}, \mathbf{s}, \mathbf{t})_l$ be the outward unit vector normal to the l-th boundary, and let the unit vector be tangent to the l-th boundary with the convention that the interior of the volume always lies on the left-hand side of the boundary. If $\theta^{(z)}$ and $\theta^{(y)}$ are defined as rotational angles about the z and y axes, respectively, it can be shown that the Eq. (14) becomes

$$\mathbf{U}_{i,j,k}^{n+1} = \mathbf{U}_{i,j,k}^{n} - \frac{\triangle t}{V_{i,j,k}} \sum_{l=1}^{N} \mathbf{R}_l^{-1} \mathbf{F}_{T_l}^{n} \triangle S_l, \tag{21}$$

where

$$\mathbf{U}_{i,j,k} = \begin{pmatrix} \rho \\ \rho u \\ \rho v \\ \rho w \\ \rho E \end{pmatrix}_{i,j,k},$$

$$\mathbf{F}_l = \begin{pmatrix} \rho u_n \\ \rho u_n^2 + \frac{1}{\gamma M^2} p \\ \rho u_n u_s \\ \rho u_n u_t \\ \left(\rho E + \frac{1}{\gamma M^2} p\right) u_n \end{pmatrix}_l, \quad \mathbf{F}_{v_l} = \frac{1}{\mathrm{Re}} \begin{pmatrix} 0 \\ \Pi_{nn} \\ \Pi_{ns} \\ \Pi_{nt} \\ \Pi_{nn} u_n + \Pi_{ns} u_s + \Pi_{nt} u_t + \frac{1}{\mathrm{EcPr}} Q_n \end{pmatrix}_l,$$

and $\mathbf{R}_l$ is the rotation matrix, given as

$$\mathbf{R} = \mathbf{R}^{(y)} \mathbf{R}^{(z)},$$

where

$$\mathbf{R}^{(y)} = \begin{pmatrix} 1 & 0 & 0 & 0 & 0 \\ 0 & \cos\theta^{(y)} & 0 & \sin\theta^{(y)} & 0 \\ 0 & 0 & 1 & 0 & 0 \\ 0 & -\sin\theta^{(y)} & 0 & \cos\theta^{(y)} & 0 \\ 0 & 0 & 0 & 0 & 1 \end{pmatrix},$$

$$\mathbf{R}^{(z)} = \begin{pmatrix} 1 & 0 & 0 & 0 & 0 \\ 0 & \cos\theta^{(z)} & \sin\theta^{(z)} & 0 & 0 \\ 0 & -\sin\theta^{(z)} & \cos\theta^{(z)} & 0 & 0 \\ 0 & 0 & 0 & 1 & 0 \\ 0 & 0 & 0 & 0 & 1 \end{pmatrix}.$$

As in the two-dimensional case, the components of the tensor in the (x, y, z) coordinates ($\mathbf{\Pi}$) are related to the components of the tensor in the (n, s, t) coordinates ($\tilde{\mathbf{\Pi}}$) through the transformation law (20).

4.4. *Time-Step and Numerical Boundary Conditions*

It turns out that for the generalized hydrodynamic equations, the stability condition

$$\triangle t = \mathrm{CFL} \cdot \min(\triangle t_1, \triangle t_2), \tag{22}$$

where

$$\triangle t_1 = M\left[\frac{\triangle x}{|a|} + \frac{2\eta M}{\rho a^2}\right],$$

$$\triangle t_2 = M\left[\frac{|a|}{\triangle x} + \frac{\eta M}{\rho \triangle x^2}\right]^{-1}$$

works well for upwind schemes. Notice that the Mach number appears in these relations. The reason is that the characteristic speed in dimensionless form becomes a/M instead of a.

For given T_w, T_r, u_w, u_r, and p_r, Eqs. (11) and (12) and the mechanical balance condition (zero normal gradient of pressure) yield the boundary values of temperature, tangential velocity, and pressure. From these values the boundary value of the density can be determined by the perfect gas relation. The velocity normal to the surface can be assumed to be zero. For artificial boundaries, inflow and outflow conditions based on the number of Euler characteristics can be employed.

4.5. *Numerical Implementation*

The discretized form of the governing generalized hydrodynamic equations in the finite volume formulation (19) or (21), a time-step restriction (22), and the boundary conditions (11) and (12) are the basic building blocks of the present numerical method. It resembles numerical methods for the compressible Navier–Stokes equations in that they all share the hyperbolic conservation laws. The present scheme, however, differs from the latter methods in the manner of calculating the viscous flux. The viscous terms in the Navier–Stokes equations can be expressed in a linear combination of entries in the Hessian-like

matrix $\nabla(\eta\nabla u)$, so that they can be transformed into an expression involving only the first derivative of u. Such a transformation cannot be applied to the generalized hydrodynamic equations because the stress is a nonlinear function of $\eta\nabla u$. The stress $\mathbf{\Pi}$ and heat flux $\mathbf{Q}$ must be retained in the discretized forms (19) and (21). The value of the stress and heat flux can be determined with the help of the Eqs. (15)–(18).

5. NUMERICAL EXPERIMENT

To demonstrate the capability of the new hydrodynamic equations, we consider two challenging problems: hypersonic shock structure and two-dimensional flat plate flow. Since our main interest lies in the development of a multidimensional computational method, the second problem will be studied in detail. The gas is assumed to be Argon (with s $= 0.75$ in the coefficient of viscosity, or $\nu = 9$, and $c = 1.0179$ [30]) in all test cases. In general, the initial data necessary to define a well-posed problem consist of dimensionless parameters (M, Kn, or Re), thermodynamic values (T_w, T_∞), gas properties (s or ν, d_{STP}), and gas–surface molecular interaction parameters (D_e, A).

5.1. *Shock Structure Problem*

Although the hypersonic shock structure problem [1, 14, 17] does not involve any solid boundary, it has been known that the numerical calculation of the shock structure presents serious theoretical and computational challenges, and the hydrodynamic approaches based on the moment methods mentioned earlier all fail to yield shock solutions beyond a relatively small value of M, typically $M \lesssim 2$. Here, the shock structure is computed for a very high Mach number ($M = 30$) with a grid of 400 points, which is illustrated in Fig. 4. The second-order accuracy was maintained in this computation. The CFL number is taken as 0.5. A steady-state solution was considered to be obtained when the rms norm for the density dropped below 10^{-8}. The general configuration of the shock structure was shown to be in good agreement with the results based on the DSMC calculation. (The reader is referred to Al-Ghoul and Eu's work based on the system of ordinary differential equations [1], where the shock solutions are shown to exist for all Mach numbers, and Myong's work of a Maxwellian gas based on the system of partial differential equations [30].) Here a calculation is presented to demonstrate that the current code has no difficulty in yielding a solution for the very high Mach numbers (up to $M = 30$) studied.

5.2. *Two-Dimensional Flat Plate Flow*

The second problem is the hypersonic rarefied flat plate flow [26, 34, 38] in which the so-called slip phenomenon is an important mechanism in determining the overall flow properties. This problem is one of fundamental interest since it generates a wide range of basic flow phenomena, for example, shock waves and slip flow.

In Figs. 5 and 6, the hypersonic rarefied flat plate flows ($M = 12.9$, Kn $= 0.0067$, $T_w = 5.4T_\infty$, $T_\infty = 200$ K) are described. The computational domain is defined by a rectangle of size 1.25×0.4 with an equally spaced grid of 120×48 points. It was checked by increasing the grid points whether the numerical results converge. Instead of the so-called Maxwell–Smoluchowski condition, a gas–surface (Ar–Al) molecular interaction model is used that depends on the pressure and temperature and provides the boundary values of

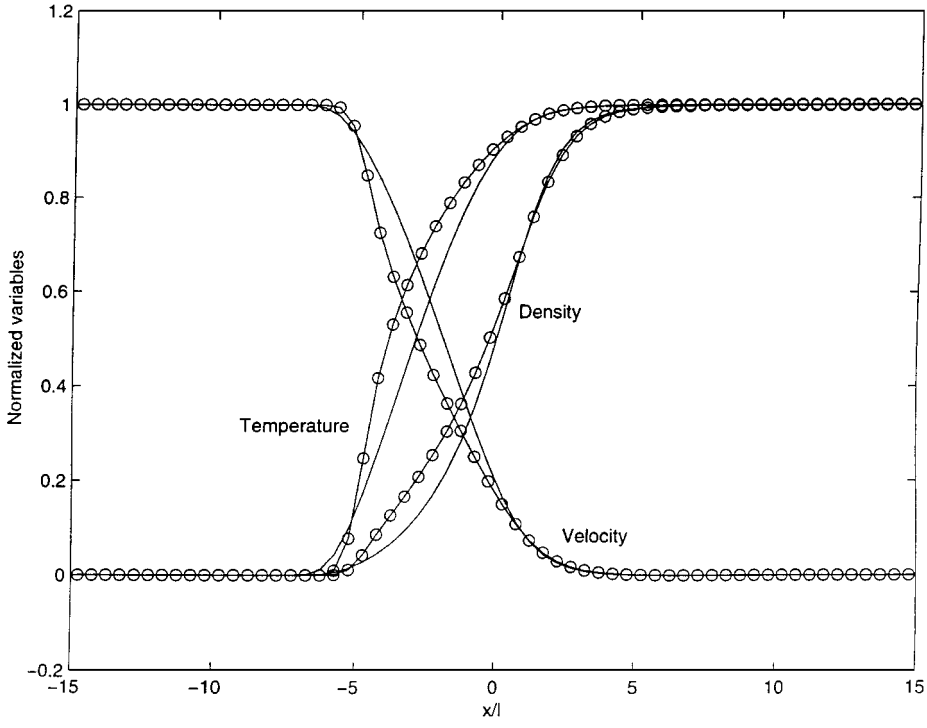

FIG. 4. Mach 30 shock profiles of normalized variables for argon gas. Normalized variables are based on the upstream and downstream states. For example, the normal density is defined as $(\rho - \rho_1)/(\rho_2 - \rho_1)$ where the subscripts 1 and 2 represent the upstream and downstream states, respectively. Solid line with circles: generalized hydrodynamics (GH); solid line: Navier–Stokes (NS). The horizontal axis represents the spatial coordinate reduced by the mean free path (l) at the upstream condition. The inverse of the shock density thickness (GH $-$ 0.1743, NS $-$ 0.2152).

temperature and velocity. The free-stream mean free path is taken as a mean collision distance. The mirror boundary before the wall was introduced to prevent the disturbance affecting the inflow boundary. The boundary condition at the outflow was specified by extrapolation. The slip condition on the wall was applied by defining the dual ghost cells, one for the inviscid part where the boundary values of velocity and temperature are specified, and another for the viscous part where the values at the wall are used. Due to the large difference between the wall and free-stream temperature, a relatively small CFL number 0.1 is used. Since our main goal is to develop a multidimensional numerical method for Eu's generalized hydrodynamic equations, for simplicity only first-order accuracy was maintained throughout the computational domain including the boundaries. More study will be needed on the second-order-accuracy upgrade and effects of boundary conditions. Exactly the same conditions, including the slip boundary condition, are applied to both Navier–Stokes and generalized hydrodynamics codes.

Numerical experiments indicated that the computing time of the two-dimensional generalized hydrodynamics code is comparable to that of the Navier–Stokes code. The excess load, which is caused by the addition of a few iterations of constitutive relations (less than 10 in most cases), occupies a small fraction of computing time in the code.

The general flow properties illustrated in Figs. 5 and 6 are qualitatively similar to the result [38] based on the DSMC calculation. The contours of density show the separation of

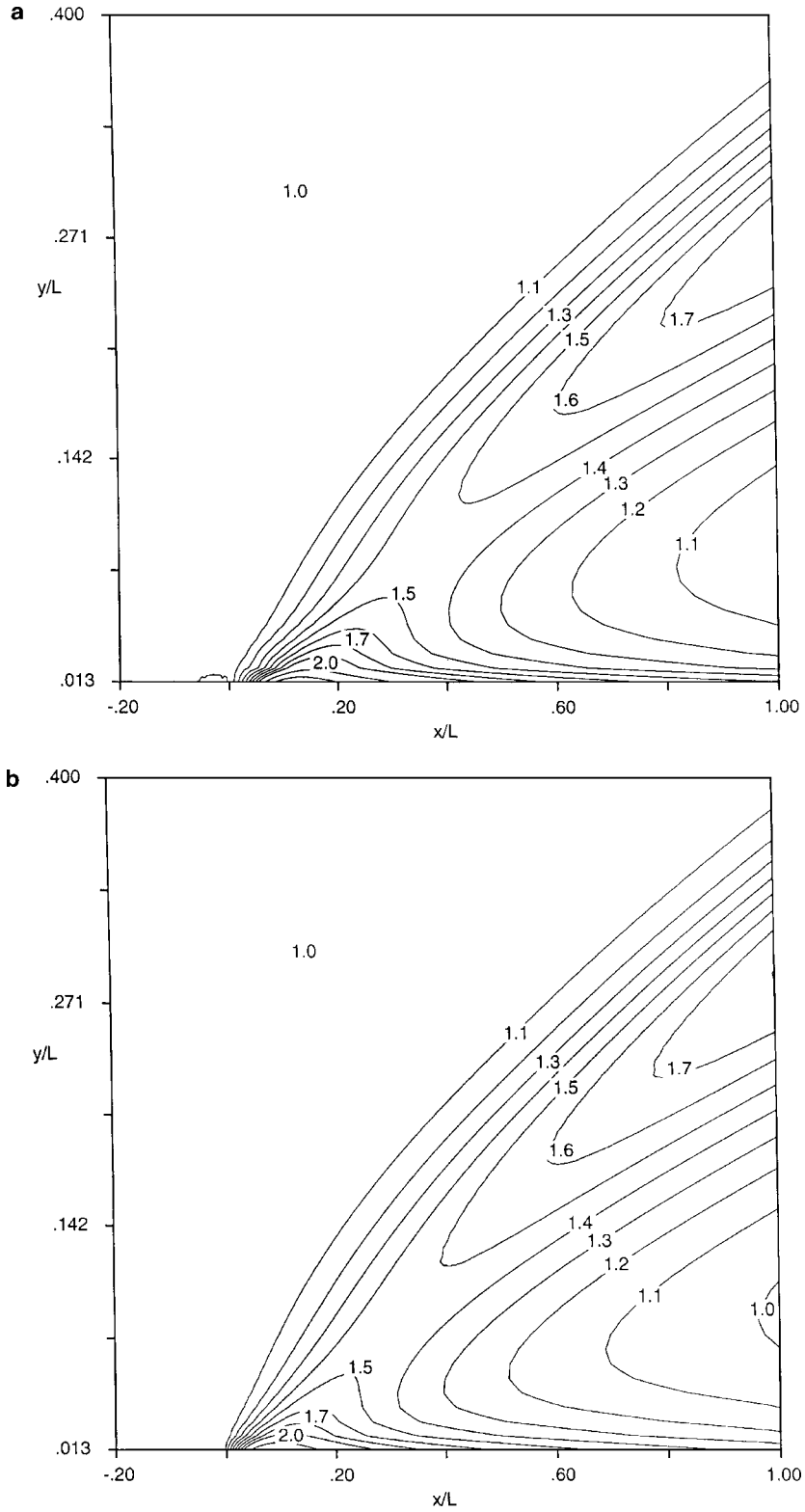

FIG. 5. Contours of constant density. (a) Generalized hydrodynamics; (b) Navier–Stokes. The solid wall begins at $x/L = 0$, where L is the length of the plate ($L = 150l_\infty$).

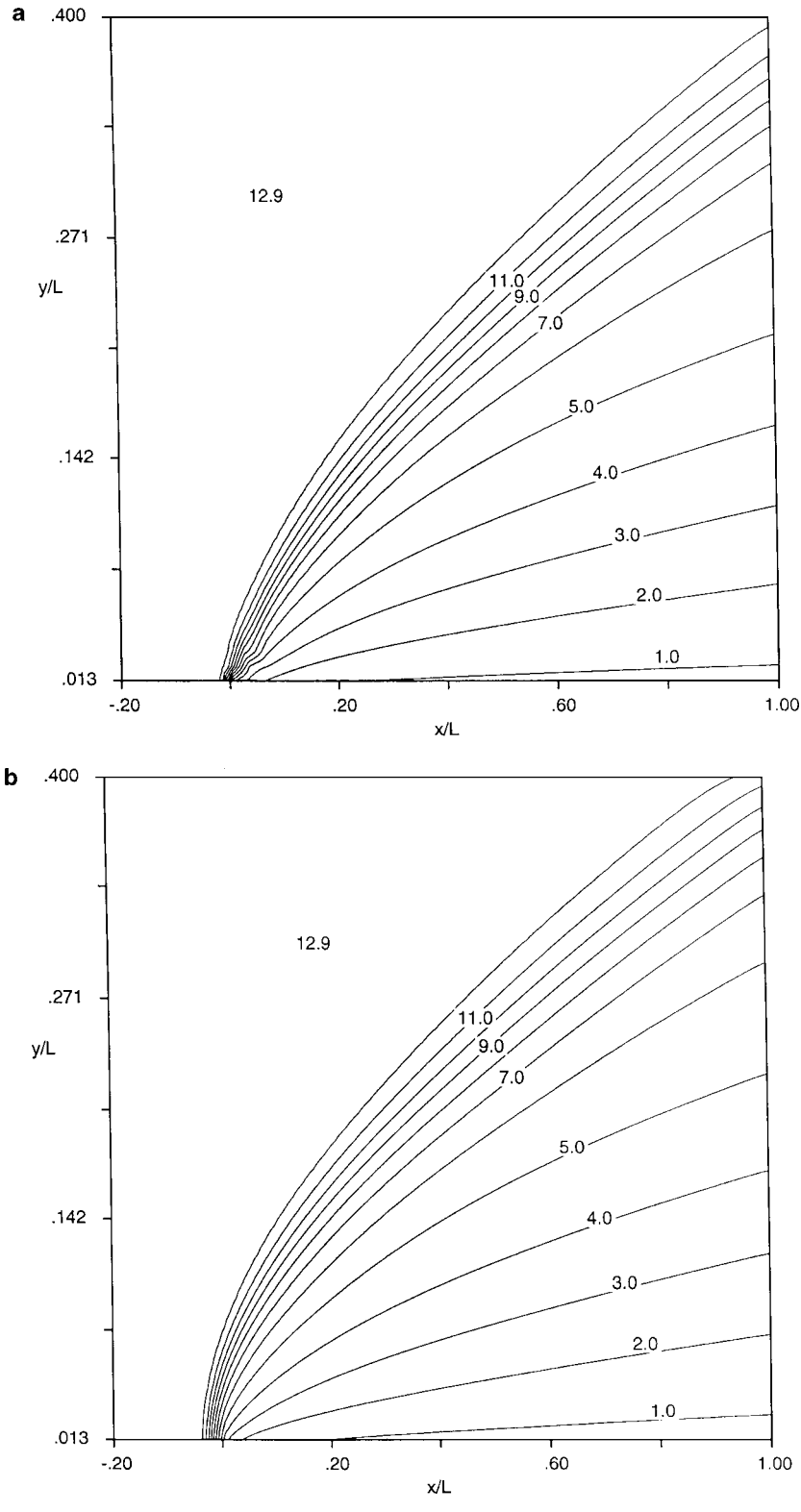

FIG. 6. Contours of Mach number. (a) Generalized hydrodynamics; (b) Navier–Stokes. The solid wall begins at $x/L = 0$, where L is the length of the plate ($L = 150l_\infty$).

the oblique shock wave and the boundary layer. The density increases across the shock, but it then decreases. The maximum line of density can be observed in both Navier–Stokes and generalized hydrodynamics results. The Mach contours show that the velocity slip is large near the leading edge and becomes small in the latter half of the plate. The slip is slightly larger in the case of generalized hydrodynamics. It can be also seen that the generalized hydrodynamics results are less smooth near the leading edge than the Navier–Stokes results. This may be because the high gradient surface in the case of generalized hydrodynamics is not well aligned with the grid lines. Finally, some interesting results can be found from the comparison between Navier–Stokes and generalized hydrodynamics calculations. As seen in Fig. 7, the Navier–Stokes calculation shows a singularity near the leading edge of the flat plate and yields a larger skin friction and heat flux. Conversely, the generalized hydrodynamics calculation removes the singularity, which appears in the case of the Navier–Stokes theory, and yields a smaller skin friction and heat flux. It should be noted that the DSMC result is similar to the present generalized hydrodynamics result in the qualitative features of the numerical results.

5.3. *Validation Issues*

The present results can be compared with the previous theoretical prediction by the DSMC or experimental data. The validation process [31] in the present work, which concerns the assessment of the accuracy of a computational simulation by comparison with experimental data, is done largely in the qualitative aspects, but not at the level of validation quantification. This is because of the uncertainties involving modeling parameters such as the type of gases, the type of slip boundary conditions, the values of accommodation coefficients, components of the wall material, etc., and also because of the lack of information on the estimates of experimental uncertainty. It remains to be seen how these parameters can affect the outcome.

With this restriction, a graphical comparison of the Navier–Stokes, generalized hydrodynamics, DSMC, and free-molecular solutions is given in Fig. 8. The distribution of shear stress Π_{xy} is plotted along the flat plate. The Maxwell–Smoluchowski boundary condition with the complete diffuse wall and the hard sphere particle model were used in the DSMC result of Yasuhara *et al.* [38]. The shear stress in the generalized hydrodynamics and DSMC increases over the first several mean free paths and peaks at about 10 mean free paths from the leading edge. It then decreases over the next 20–30 mean free paths and approaches an asymptotic value at the end of the plate. Such a trend can be found also in experimental data [23]. In contrast to this result, the shear stress in the Navier–Stokes solutions reaches the peak immediately, which is a sign of singularity in the continuum limit, and then declines sharply in the aft part of the plate. The magnitude of the peak in the shear stress is considerably larger than that of the DSMC method.

Since this difference of the generalized hydrodynamics from the Navier–Stokes theory with regard to the existence of singularity in the shear stress near the leading edge is consistent in the DSMC method, it can be concluded that the generalized hydrodynamic equations remove the continuum singularity in gas flows of the flat plate. The ultimate reason for this can be traced to the fact that through the relations (2) and (3) the stress is nonlinearly related to the gradient of velocity in high nonequilibrium regions. As can be seen in Fig. 3b, the behavior of shear stress becomes very different from the Navier–Stokes description in highly nonequilibrium states, approaching zero as the velocity gradient increases. It is this non-Newtonian effect that allows the gradual increase of the shear stress near the leading

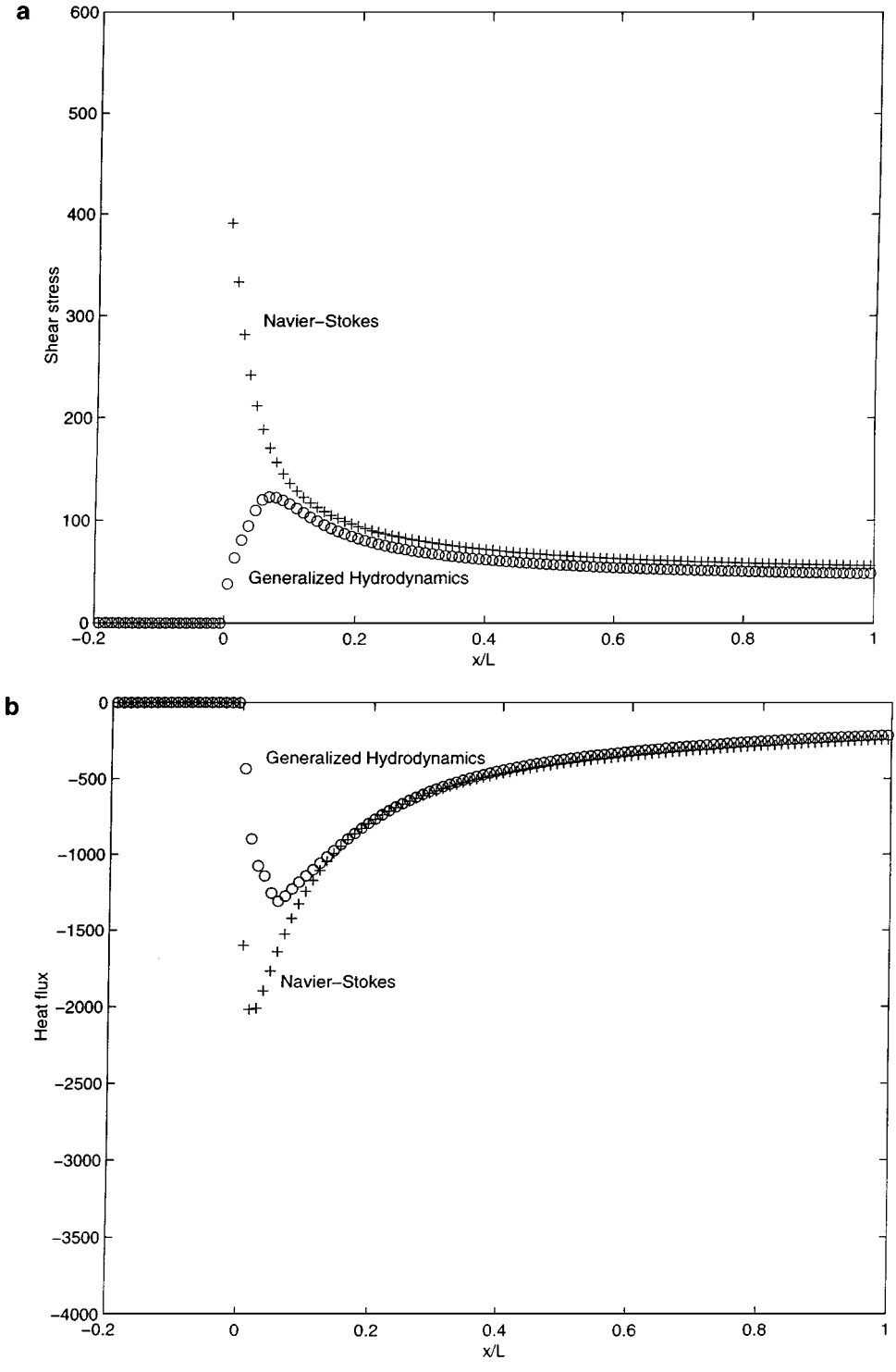

FIG. 7. Properties near the plate. (a) Shear stress Π_{xy}, (b) heat flux Q_y. The solid wall begins at $x/L = 0$.

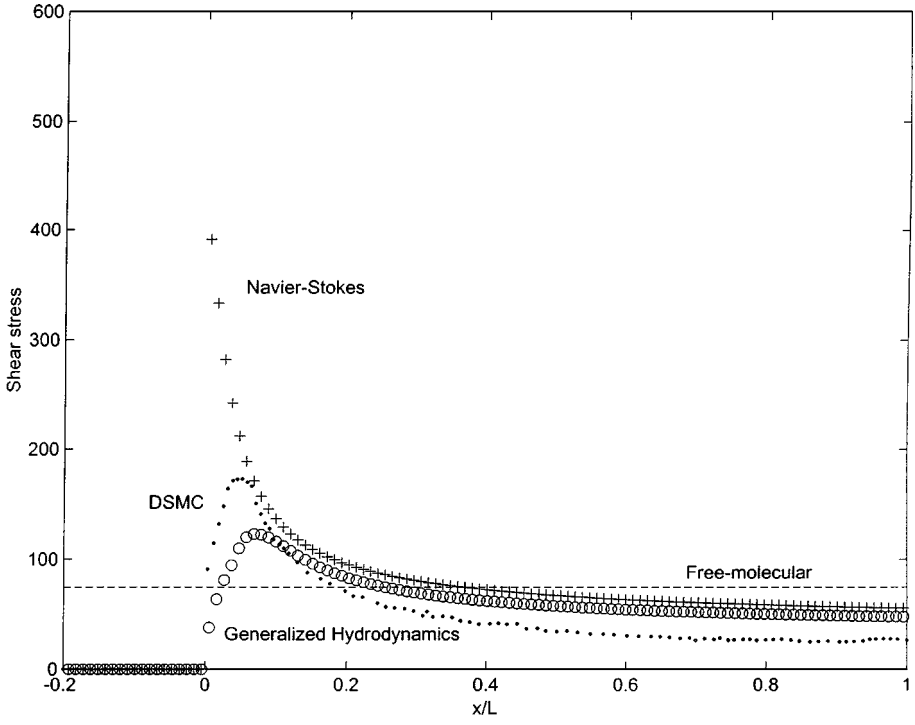

FIG. 8. Comparison of shear stresses Π_{xy} along surface predicted by the Navier–Stokes, generalized hydrodynamics, DSMC, and free-molecular theory. The solid wall begins at $x/L = 0$.

edge where a very high velocity gradient arising from the presence of the solid wall is always observed. However, the shear stress in the Navier–Stokes solutions will reach the peak right at the leading edge where the velocity gradient becomes maximum.

6. CONCLUSIONS

As a step toward developing reliable high-order fluid dynamic computational models for rarefied and microscale gas flows, Eu's generalized hydrodynamic equations have been numerically studied. The numerical results obtained by using a multidimensional computational method are presented. The main emphasis is placed on the development of a multidimensional finite-volume method for the highly nonlinear generalized hydrodynamic equations of Eu. The new equation is shown to yield solutions in rarefied hypersonic gas flow over a flat plate in which the singularity in the continuum limit does not appear.

The motivation of this study was to demonstrate a possibility of using Eu's generalized hydrodynamics as the basis of a multidimensional computational method of rarefied and microscale gasdynamics. There can be many alternatives to the numerical method taken in the present study. In particular, a numerical method which can deal with the stiffness problem in calculating low Mach number flows will become essential when one tries to solve low-speed microscale gas flows.

Extension to more complicated gases will present nontrivial challenges. For example, the rotational nonequilibrium effect in diatomic gases will make the constitutive equations more complicated. It is also expected that the work involving a gas mixture will become

considerably complicated, but the same algorithms should be applicable. The results of studies of these problems will be reported in due course.

ACKNOWLEDGMENTS

This work was supported by the Korea Science and Engineering Foundation under Research Grant 1999-2-305-001-3. Part of this work was performed while the author was a visitor at the Institute for Mathematics and Its Applications, University of Minnesota (1999–2000 Program: Reactive Flow and Transport Phenomena). The author thanks the Institute for the hospitality extended during his stay and expresses his deep appreciation to Professor B. C. Eu for his encouragement and advice.

REFERENCES

1. M. Al-Ghoul and B. C. Eu, Generalized hydrodynamics and shock waves, *Phys. Rev. E* **56**(3), 2981 (1997).
2. E. B. Arkilic, M. A. Schmidt, and K. S. Breuer, Gaseous slip flow in long microchannels, *IEEE J. MEMS* **6**(2), 167 (1997).
3. R. Balakrishnan, R. K. Agarwal, and K. Y. Yun, *High-order Distribution Functions, BGK-Burnett Equations and Boltzmann's H-theorem*, Technical Paper 97-2551 (AIAA Press, Washington DC, 1997).
4. A. Beskok and G. E. Karniadakis, A model for flows in channels, pipes, and ducts at micro and nano scales, *Microscale Thermophys. Eng.* **3**, 43 (1999).
5. D. K. Bhattacharya and B. C. Eu, Nonlinear transport processes and fluid dynamics: Effects of thermoviscous coupling and nonlinear transport coefficients on plane Couette flow of Lennard–Jones fluids, *Phys. Rev. A* **35**(2), 821 (1987).
6. G. A. Bird, *Molecular Gas Dynamics and the Direct Simulation of Gas Flows* (Clarendon Press, Oxford, England, 1994).
7. S. Brown, *Approximate Riemann Solvers for Moment Models of Dilute Gases*, Ph.D. thesis (The University of Michigan, 1996).
8. S. Chapman and T. G. Cowling, *The Mathematical Theory of Nonuniform Gases*, 3rd ed. (Cambridge Univ. Press, London, 1970).
9. K. A. Comeaux, D. R. Chapman, and R. W. MacCormack, *An Analysis of the Burnett Equations Based on the Second Law of Thermodynamics*, Technical Paper 95-0415 (AIAA Press, Washington, DC, 1995).
10. B. C. Eu, A modified moment method and irreversible thermodynamics, *J. Chem. Phys.* **73**(6), 2958 (1980).
11. B. C. Eu, On the corotating frame and evolution equations in kinetic theory, *J. Chem. Phys.* **82**(8), 3773 (1985).
12. B. C. Eu, *Kinetic Theory and Irreversible Thermodynamics* (Wiley, New York, 1992).
13. B. C. Eu, *Nonequilibrium Statistical Mechanics. Ensemble Method* (Kluwer Academic Publishers, Dordrecht, 1998).
14. K. A. Fiscko and D. R. Chapman, Comparison of Burnett, super-Burnett and Monte Carlo solutions for Hypersonic Shock Structure, *Prog. Astronaut. Aeronaut.* **118**, 374 (1989).
15. A. M. Goodbody, *Cartesian Tensors: With Applications to Mechanics, Fluid Mechanics and Elasticity* (Ellis Horwood Ltd., Chichester, England, 1982).
16. H. Grad, On the kinetic theory of rarefied gases, *Comm. Pure Appl. Math.* **2**, 331 (1949).
17. H. Grad, The profile of a steady plane shock wave, *Comm. Pure Appl. Math.* **5**, 257 (1952).
18. H. Haken, *Synergetics* (Springer-Verlag, Berlin, 1977), p. 202.
19. C. M. Ho and Y. C. Tai, Micro-electro-mechanical-systems (MEMS) and fluid flows, *Annu. Rev. Fluid Mech.* **30**, 579 (1998).
20. M. S. Ivanov and S. F. Gimelshein, Computational hypersonic rarefied flows, *Annu. Rev. Fluid Mech.* **30**, 469 (1998).
21. J. Koplik and J. R. Banavar, Continuum deductions from molecular hydrodynamics, *Annu. Rev. Fluid Mech.* **27**, 257 (1995).

22. C. J. Lee, Unique determination of solutions to the Burnett equations, *AIAA J.* **32**(5), 985 (1994).
23. J. C. Lengrand, J. Allègre, and A. Chpoun, Rarefied hypersonic flow over a sharp flat plate: Numerical and experimental results, *Prog. Astronaut. Aeronaut.* **160**, 276 (1992).
24. C. D. Levermore, Moment closure hierarchies for kinetic theories, *J. Stat. Phys.* **83**, 1021 (1996).
25. C. D. Levermore and W. J. Morokoff, The Gaussian moment closure for gas dynamics, *SIAM J. Appl. Math.* **59**(1), 72 (1998).
26. R. G. Lord, Direct simulation of rarefied hypersonic flow over a flat plate with incomplete surface accommodation, *Prog. Astronaut. Aeronaut.* **160**, 221 (1992).
27. F. E. Lumpkin, III, I. D. Boyd, and E. Venkatapathy, *Comparison of Continuum and Particle Simulations of Expanding Rarefied Flows*, Technical Paper 93-0728 (AIAA Press, Washington, DC, 1993).
28. I. Müller and T. Ruggeri, *Extended Thermodynamics* (Springer-Verlag, New York, 1993).
29. R. S. Myong, *A New Hydrodynamic Approach to Computational Hypersonic Rarefied Gasdynamics*, Technical Paper 99-3578 (AIAA Press, Washington, DC, 1999).
30. R. S. Myong, Thermodynamically-consistent hydrodynamic computational models for high-Knudsen-number gas flows, *Phys. Fluids* **11**(9), 2788 (1999).
31. W. L. Oberkampf and T. G. Trucano, *Validation Methodology in Computational Fluid Dynamics*, Technical Paper 2000-2549 (AIAA Press, Washington, DC, 2000).
32. E. S. Oran, C. K. Oh, and B. Z. Cybyk, Direct simulation Monte Carlo: Recent advances and applications, *Annu. Rev. Fluid Mech.* **30**, 403 (1998).
33. R. Roveda, D. B. Goldstein, and P. L. Varghese, Hybrid Euler/particle approach for continuum/rarefied flows, *J. Spacecraft Rockets* **35**(3), 258 (1998).
34. J. C. Tannehill and R. A. Mohling, *Numerical Computation of the Hypersonic Rarefied Flow Near the Sharp Leading Edge of a Flat Plate*, Technical Paper 73-200 (AIAA Press, Washington, DC, 1973).
35. B. van Leer, *Flux-vector Splitting for the Euler Equations*, Technical Report ICASE 82-30 (NASA Langley Research Center, 1982).
36. B. van Leer, On the relation between the upwind-differencing schemes of Godunov, Enguist-Osher and Roe, *SIAM J. Sci. Stat. Comput.* **5**(1), 1 (1985).
37. L. C. Woods, Frame-indifferent kinetic theory, *J. Fluid Mech.* **136**, 423 (1983).
38. M. Yasuhara, Y. Nakamura, and J. Tanaka, Monte Carlo simulation of flow into channel with sharp leading edge, *Prog. Astronaut. Aeronaut.* **118**, 582 (1989).